Mon. Not. R. Astron. Soc. **000**, 000–000 (0000) Printed 5 February 2008 (MN LATEX style file v2.2)

Integrated-light *VRI* imaging photometry of globular clusters in the Magellanic clouds

Paul Goudfrooij,[1⋆] Diane Gilmore,[1] Markus Kissler-Patig,[2]†and Claudia Maraston[3]

[1] *Space Telescope Science Institute, 3700 San Martin Drive, Baltimore, MD 21218, U.S.A.*
[2] *European Southern Observatory, Karl-Schwarzschild-Strasse 2, D-85748 Garching bei München, Germany*
[3] *University of Oxford, Astrophysics, Denys Wilkinson Building, Keble Road, Oxford OX1 3RH, United Kingdom*

Accepted 2006 March 14. Received 2006 March 13; in original form 2006 February 14

ABSTRACT

We present accurate integrated-light photometry in Johnson/Cousins V, R, and I for a sample of 28 globular clusters in the Magellanic Clouds. The majority of the clusters in our sample have reliable age and metallicity estimates available in the literature. The sample encompasses ages between 50 Myr and 7 Gyr, and metallicities ([Fe/H]) between -1.5 and 0.0 dex. The sample is dominated by clusters of ages between roughly 0.5 and 2 Gyr, an age range during which the bolometric luminosity of simple stellar populations is dominated by evolved red giant branch stars and thermally pulsing asymptotic giant branch (TP-AGB) stars whose theoretical colours are rather uncertain. The *VRI* colours presented in this paper have been used to calibrate stellar population synthesis model predictions.

Key words: Magellanic Clouds, techniques: photometric, galaxies: evolution, galaxies: star clusters

1 INTRODUCTION

One of the predictions of stellar evolution theory is that evolved red giant stars dominate the bolometric luminosity of a simple stellar population (SSP) after a few hundred million years. According to predictions based on canonical stellar models (Renzini & Buzzoni 1986), the first (and sudden) appearance of a prominent red stellar sequence is that of bright Asymptotic Giant Branch (AGB) stars followed by the development of the Red Giant Branch (RGB), both occurring before an age of 1 Gyr. The onset of the RGB is predicted to occur at an age of about 0.6 Gyr (Renzini & Buzzoni 1986) and observational efforts have verified this prediction (e.g., Ferraro et al. 1995, 2004). However, theoretical modelling of the AGB phase is rather complicated. For example, strong and poorly constrained mass loss and envelope burning affect stellar evolution through the AGB phase (e.g., Iben & Renzini 1983; Wagenhuber & Groenewegen 1998; Girardi & Bertelli 1998; Marigo 2001). These phenomena hamper a straightforward theoretical prediction of lifetimes and effective temperatures during the thermally-pulsing part of the AGB phase (the so-called TP-AGB phase). Hence, an empirical calibration of the colours of SSPs during this age range is important (see also Renzini 1992; Maraston 1998).

The globular cluster system of the Magellanic Clouds provides a unique opportunity to study the influence of the AGB phase to the spectral energy distribution of SSPs as a function of age and chemical composition. Globular clusters in the Magellanic Clouds cover a wide range in age and metallicity, and clusters with ages between 0.1 and 2 Gyr are present in significant numbers (e.g., Searle, Wilkinson, & Bagnuolo 1980; Elson & Fall 1985; Sagan & Pandey 1989; Frogel, Mould, & Blanco 1990; Girardi et al. 1995). Maraston (1998) presented SSP models whose calibration matches the energetics and colours of globular clusters in the Magellanic Clouds. The onset of the TP-AGB phase occurs at $\sim$0.2 Gyr and lasts until $\sim$2 Gyr. During this age range, TP-AGB stars dominate the near-IR and even the bolometric light of SSPs (Maraston 1998).

The age range of $0.2 - 2$ Gyr, during which AGB stars are expected to dominate the light, is of strong interest and significance to several popular topics in present-day astronomy and astrophysics. For example, it is similar to the crossing time of galaxy-sized stellar systems, which is a measure of the formation timescale of a galaxy. Modern observational facilities like the *Hubble Space Telescope (HST)*, the *Spitzer Space Telescope* and 10-m-class ground-based telescopes have been able to identify various populations of faint galaxies at high redshift ($z \gtrsim 1$), for which the accuracy of

⋆ E-mail (internet): goudfroo@stsci.edu
† Visiting Astronomer, Cerro Tololo Inter-American Observatory. CTIO is operated by the Association of Universities for Research in Astronomy (AURA), Inc., under contract to the U. S. National Science Foundation.

age determination is relevant to testing the predictions of various galaxy formation scenarios (see also Maraston 2004). This age range is also very relevant to the identification and study of post-starburst galaxies and merger remnants (e.g., Whitmore et al. 1993; Schweizer et al. 1996; Maraston et al. 2001; Goudfrooij et al. 2001a,b, and references therein).

The models by Maraston (1998) were calibrated in the U, B, V, J, H, and K passbands. In order to allow for a wider calibration of SSP models, we have obtained integrated-light photometry in the V, $R_{\rm KC}$, and $I_{\rm KC}$ bands of 28 clusters in the Large and Small Magellanic Clouds (hereafter LMC and SMC). We use digital CCD imaging and employ a range of aperture sizes in order to evaluate the aperture size dependence of cluster colours and their uncertainties. In contrast, virtually all previous studies used single-aperture photometry or photographic plates.

Our photometry has already been used by Maraston (2005) for calibrating her SSP models in the full wavelength range from U to K. The influence of TP-AGB stars are found to be significant in both the R and I passbands (cf. Fig. 19 in Maraston 2005). In this paper we present the full data set.

To our knowledge, this is the first study to present integrated magnitudes in the R– and I bands for *any* LMC globular cluster and for several SMC globular clusters as well. Among the Johnson-Kron-Cousins passbands in the optical, R and I are most affected by the AGB phase of stellar evolution. Hence, a calibration of these passbands are important for proper identification of faint young galaxies at cosmological redshifts ($1 \lesssim z \lesssim 6$) through photometric redshift and spectral energy distribution studies in the near-IR and mid-IR.

1.1 Sample selection

Taking the sample of bright globular clusters studied by Frogel et al. (1990) as a starting point, we selected a sample of star clusters with Searle, Wilkinson & Bagnuolo (1980, hereafter SWB) types between III and VI with the purpose to select clusters in the age range of $0.3 \lesssim t \lesssim 2$ Gyr (e.g., Frogel et al. 1990), which is relevant to constraining the influence of AGB stars on the integrated colours of stellar populations. Care was taken to select a suitably high and approximately equal number of clusters in each SWB type between III and VI. As individual clusters have masses of a few $10^4 M_\odot$ and lifetimes of luminous AGB stars are quite short ($\lesssim 10^7$ yr), stochastic fluctuations strongly affect the observed number of AGB stars per cluster (see also Maraston 1998; Bruzual & Charlot 2003). Hence, the selection of several clusters in each SWB type allows one to set empirical constraints on such stochastic effects as a function of age. Relevant global parameters of the star clusters in our sample are listed in Table 1.

2 OBSERVATIONS AND BASIC DATA REDUCTION

Observations were performed during two runs at the 0.9-m telescope of Cerro Tololo Interamerican Observatory (CTIO) in f/13.5 mode using the CCD imager and a dedicated 2048x2048 SITe CCD, which was employed in gain setting 2 (1.5 e^-/ADU), yielding a read noise of 3.6 e^- per pixel. With a plate scale of $0\farcs40$ pixel^{-1}, the field of view is $13\farcm6 \times 13\farcm6$. Images were taken through Johnson V and Kron-Cousins R and I filters. Other details on the observation runs are listed in Table 2.

Bias and dome flat images as well as images of the sky during twilight ("sky flats") were acquired daily and used for basic CCD calibration using the CCDPROC package of IRAF. During acquisition of the sky flat frames, care was taken to acquire several images per filter with 10-arcsecond offsets of the telescope between images so that any stars in the field as well as bad pixels and cosmic ray hits could be eliminated during image combination and smooth illumination correction frames could be created. Standard star fields from Landolt (1992) with an appropriate range of intrinsic colours were observed several times per night to derive photometric transformation equations and extinction corrections. Typically, a total of three or four standard star fields were observed two or three times each per night. The log of Magellanic cloud star cluster observations is listed in Table 3.

Each target globular cluster was centered roughly 2 arcmin away from the centre of the CCD in order to maximize the area usable for the determination of the background level (see Sect. 3 below), yet still cover the full spatial extent of the target clusters. Multiple exposures were taken through each filter. The telescope was offset by 5 arcsec between each exposure, which facilitated the elimination of cosmic ray hits and hot pixels during image combination. The latter was done using IRAF task IMCOMBINE using the CRREJECT option after having aligned the subimages in each filter to a common coordinate system using centroids of relatively isolated stars in the field. The alignment accuracy was always better than 0.05 pixels in each axis.

The weather during the January 2002 run was photometric, and the photometric zeropoint calibrations stayed constant throughout that run to within 0.01 mag. The December 2004 run, which was performed in service mode operated by the SMARTS[1] consortium, suffered from non-photometric weather. The photometric transformation equations for these images were derived by comparing observed count rates of several tens of stars in the field of view of each cluster image with V and I-band photometry published by Zaritsky et al. (2002; 2004) and R-band photometry by Massey (2002) as follows. We first selected stars from the Zaritsky et al. and Massey catalogs with celestial positions between 3 and 10 arcmin away from the cluster centre positions. The latter were taken from Bica et al. (1999) for the LMC clusters and Welch (1991) for the SMC clusters. (The inner radius threshold of 3 arcmin was put in place to avoid the crowded areas near the cluster centres.) The astrometric zeropoint offset between the Zaritsky et al. and Massey catalogs and the world coordinate system of our images was determined for each cluster by identifying (by eye, using the ESO SKYCAT tool) a star in those catalogs located near the centre of our image and measuring the pixel location of the centroid of that star on our image. Estimated pixel positions of all other stars (selected as mentioned above) around the

[1] Small and Moderate Aperture Research Telescope System, see http://www.astro.yale.edu/smarts

Table 1. General properties of globular clusters in our sample.

Cluster ID (1)	RA J2000 (2)	DEC J2000 (3)	SWB Type (4)	Log (Age) [yr] (5)	Age Ref. (6)	[Fe/H] [dex] (7)	[Fe/H] Ref. (8)	A_V [mag] (9)	$\sigma(A_V)$ [mag] (10)
				SMC Clusters					
Kron 3	00 24 44	−72 47 20	VI–VII	$9.78^{+0.09}_{-0.11}$	1	-1.16 ± 0.09	1	0.18*	0.02
NGC 152	00 32 56	−73 06 57	IV	$9.15^{+0.06}_{-0.07}$	2	-0.94 ± 0.15	2	0.19	0.02
NGC 265	00 47 12	−73 28 38	III	8.30	3	.....		0.20	0.02
NGC 339	00 57 49	−74 28 00	VII	$9.80^{+0.08}_{-0.10}$	4	-1.50 ± 0.14	4	0.18	0.02
NGC 411	01 07 56	−71 46 05	V–VI	$9.15^{+0.06}_{-0.07}$	2,4	-0.68 ± 0.07	2,4	0.17	0.02
NGC 419	01 08 29	−72 53 12	V	$9.08^{+0.15}_{-0.23}$	5	-0.7 ± 0.3	5	0.32	0.02
				LMC Clusters					
NGC 1644	04 37 39	−66 11 58	V	8.94	6	.....		0.28*	0.02
NGC 1651	04 37 32	−70 35 06	V	$9.30^{+0.08}_{-0.10}$	7	-0.37 ± 0.20	12	0.35	0.05
NGC 1751	04 54 12	−69 48.24	VI	9.18	6	-0.18 ± 0.20	12	0.51	0.02
NGC 1755	04 55 14	−68 12 17	II	7.98	6	.....		0.55	0.02
NGC 1783	04 59 08	−65 59 20	V	9.11	6	-0.45 ± 0.03	13	0.31	0.02
NGC 1806	05 02 11	−67 59 20	V	8.70	8	-0.23 ± 0.20	12	0.25	0.04
NGC 1831	05 06 16	−64 55 06	IV A	$8.50^{+0.30}_{-0.30}$	9	$+0.01 \pm 0.20$	12	0.39*	0.02
NGC 1846	05 07 35	−67 27 39	VI	9.08	6	-0.70 ± 0.20	12	0.45	0.03
NGC 1866	05 13 39	−65 27 54	III	$8.12^{+0.30}_{-0.30}$	9	-0.50 ± 0.10	14	0.26	0.03
NGC 1868	05 14 36	−63 57 18	IV A	$8.74^{+0.30}_{-0.30}$	9	-0.50 ± 0.20	12	0.39*	0.02
NGC 1978	05 28 45	−66 14 12	VI	$9.30^{+0.05}_{-0.05}$	7	-0.42 ± 0.20	12	0.55	0.03
NGC 1987	05 27 17	−70 44 06	IV B	8.79	6	.....		0.33	0.03
NGC 2058	05 36 54	−70 09 44	III	8.06	6	.....		0.24	0.02
NGC 2134	05 51 56	−71 05 51	III	8.28	6	−1.0	15	0.49	0.02
NGC 2136	05 53 17	−69 31 42	III	$8.00^{+0.10}_{-0.10}$	8	-0.55 ± 0.23	8	0.46	0.02
NGC 2154	05 57 38	−67 15 43	V	9.01	6	-0.56 ± 0.20	12	0.34	0.02
NGC 2155	05 58 33	−65 28 36	VI	$9.51^{+0.06}_{-0.07}$	10	-0.55 ± 0.20	12	0.35	0.03
NGC 2162	06 00 31	−63 43 18	V	$9.11^{+0.12}_{-0.16}$	7	-0.23 ± 0.20	12	0.39	0.02
NGC 2164	05 58 54	−68 31 06	II	$7.70^{+0.20}_{-0.20}$	11	-0.60 ± 0.20	16	0.41	0.07
NGC 2173	05 57 58	−72 58 42	VI	$9.33^{+0.07}_{-0.09}$	7	-0.24 ± 0.20	12	0.39*	0.02
NGC 2213	06 10 42	−71 31 42	V	$9.20^{+0.10}_{-0.12}$	7	-0.01 ± 0.20	12	0.44	0.02
NGC 2231	06 20 44	−67 31 06	V	$9.18^{+0.10}_{-0.13}$	7	-0.67 ± 0.20	12	0.39	0.02

Notes to Table 1. Column (1): Cluster ID. Columns (2) and (3): Right Ascension (given as hours, minutes, and seconds) and Declination (given as degrees, arcminutes, and arcseconds)) in J2000.0 equinox, both taken from Welch (1991) for the SMC clusters and from Bica et al. (1999) for the LMC clusters. Column (4): SWB type from Frogel et al. (1990) or Bica et al. (1996). Column (5): Logarithm of age from literature. Column (6): Age reference code (see below). Column (7): [Fe/H] from literature. Column (8): [Fe/H] reference code (see below). Columns (9) and (10): Assumed foreground extinction in V-band and its uncertainty, derived from data in Zaritsky et al. (2002; 2004), made available through http://ngala.as.arizona.edu/dennis/lmcdata.html. Entries with asterisk superscript were derived using Schlegel et al. (1998). See text in Sect. 3.3.

References: (1) Mighell et al. (1998); (2) Crowl et al. (2001); (3) Maraston (2005); (4) Da Costa & Hatzidimitriou (1998); (5) Durand et al. (1984);(6) Girardi & Bertelli (1998); (7) Geisler et al. (1997); (8) Dirsch et al. (2000); (9) Elson & Fall (1988); (10) Rich et al. (2001); (11) Elson (1991); (12) Olszewski et al. (1991); (13) Cohen (1982); (14) Hill et al. (2000); (15) Hodge (1984); (16) Schommer & Geisler (1988).

cluster in question are then calculated. This list of pixel positions is subsequently used as input to the DAOPHOT-II package (Stetson 1987) as implemented within IRAF to calculate aperture photometry for those stars on our images. Comparing the input list of pixel positions with positions in the final list of instrumental magnitudes of those stars shows that the positional agreement was better than 1.5 pixels RMS in all cases, good enough to avoid confusion due to crowding. Aperture corrections are derived separately for each filter and each cluster by using curve-of-growth measurements for several isolated stars in the field. Finally, photometric transformation solutions were derived separately for each cluster observed during the Dec 2004 run. These solutions involved a zero-point term and one linear colour term (using $V-I$ for V and I and $V-R$ for R). The RMS uncertainty of these photometric solutions ranges between 0.01 and 0.04 mag, which is smaller than other sources of error in the measurement of integrated cluster colours (see below).

Table 2. Observing runs at the CTIO 0.9-m telescope.

Run	Jan 02	Dec 04
Allocation	NOAO	SMARTS
Dates	Jan 10–13, 2002	Dec 9–11, 2004
Observer	Kissler-Patig	Gomez[1]
Conditions	Photometric	Variable clouds

[1] A. Gomez, SMARTS service observer.

Table 3. Observing log

Object	Observing Date	Exposure Time (s) V	R	I	V-band seeing*
Kron 3	Dec 10, 2004	3×420	3×240	3×450	1.19
NGC 152	Jan 10, 2002	3×500	3×500	3×600	1.60
NGC 265	Jan 13, 2002	3×400	3×250	3×400	1.77
NGC 339	Dec 11, 2004	3×420	3×240	3×450	1.31
NGC 411	Dec 9, 2004	3×420	3×240	3×450	1.25
NGC 419	Jan 12, 2002	3×400	3×250	3×400	1.74
NGC 1644	Jan 10, 2002	3×200	3×200	3×400	1.47
NGC 1651	Dec 11, 2004	3×210	3×150	3×240	1.24
NGC 1751	Jan 13, 2002	3×180	3×140	3×200	1.56
NGC 1755	Jan 13, 2002	3×180	3×140	3×200	1.55
NGC 1783	Jan 12, 2002	3×180	3×140	3×200	1.50
NGC 1806	Dec 9, 2004	3×210	3×150	3×240	1.33
NGC 1831	Jan 12, 2002	3×180	3×140	3×200	1.31
NGC 1846	Jan 12, 2002	3×180	3×140	3×200	1.54
NGC 1866	Jan 10, 2002	3×300	3×250	3×500	2.02
NGC 1868	Jan 13, 2002	3×180	3×140	3×200	1.45
NGC 1978	Jan 10, 2002	3×200	3×200	3×400	1.71
NGC 1987	Jan 10, 2002	3×250	3×200	3×400	2.30
NGC 2058	Jan 13, 2002	3×180	3×140	3×200	2.12
NGC 2134	Jan 12, 2002	3×180	3×140	3×200	1.31
NGC 2136	Jan 12, 2002	3×180	3×140	3×200	1.54
NGC 2154	Jan 13, 2002	3×180	3×140	3×200	1.35
NGC 2155	Jan 12, 2002	3×180	3×140	3×200	1.77
NGC 2162	Jan 13, 2002	3×180	3×140	3×200	1.40
NGC 2164	Dec 9, 2004	3×210	3×150	3×240	1.23
NGC 2173	Jan 13, 2002	3×180	3×140	3×200	1.25
NGC 2213	Jan 12, 2002	3×180	3×140	3×200	1.92
NGC 2231	Jan 12, 2002	3×180	3×140	3×200	1.82

* Seeing FWHM values in arcsec.

3 INTEGRATED-LIGHT CLUSTER PHOTOMETRY

3.1 Measurement technique

The measurement of integrated magnitudes and colours of globular clusters in the Magellanic clouds is complicated by several factors. One problem is that of accurate centering of the measurement aperture. Many of these clusters are superposed onto a relatively high surface density of stars associated with the LMC or SMC, and some have a rather irregular star distribution and/or are not particularly symmetric due to the superposition of bright stars (be it supergiants or AGB stars within the cluster itself, those associated with the body of the LMC or SMC, or Galactic foreground stars). On the other hand, it should be recognized that the use of CCD images in this context renders these problems much less severe than they were for previous studies which used single-channel photometers and diaphragms which were centered by eye or by maximum throughput. After some experimentation, we decided to employ the following centering method for each cluster. Using the point spread function-fitting mode of the DAOPHOT-II package, we first removed stars brighter than the magnitude of an O9 supergiant star ($M_V = -6.4$, Schmidt-Kaler 1982) at the distance of the LMC or SMC (for this purpose we adopt $(m-M) = 18.24$ for the LMC and $(m-M) = 18.75$ for the SMC; Udalski 2000) from the V-band image. In order to determine a proper luminosity-weighted centre, we then convolved this image by a series of circular Gaussians with standard deviations of 20 through 60 pixels (i.e., 8 through 24 arcsec), and the centroids of the clusters (and their uncertainties) were measured for each, starting with an initial guess estimated by eye. The final cluster centre was defined as the mean centroid weighted by the inverse variances of the individual centroid fits. The standard error of the cluster centre was taken to be the standard deviation of the list of cluster centres as derived above.

Since globular clusters vary significantly in size, we chose to measure the cluster photometry using several aperture sizes, including the (typically single) aperture size used by previous studies to allow a simple comparison. The apertures are circular and the same for all filter bands. The subtraction of "background" light not belonging to the target clusters themselves (i.e., sky, Galactic foreground stars, and the diffuse stellar population associated with the LMC or SMC at the location of the target clusters) was performed as follows. We started out with the images from which single stars brighter than the equivalent of $M_V = -6.4$ were removed (see above). Areas affected by CCD saturation or obvious scattered light from internal reflections due to the presence of bright stars were also flagged and excluded from background level measurements. The mean background level (and its uncertainty) was measured from the (remaining) area on the cluster images away from the cluster centre by 3 arcmin (i.e., $\sim$40 pc) or more. In the cases where more than one cluster is present on the image (e.g., NGC 1755, NGC 2058, NGC 2065), we also excluded pixels within 3 arcmin from those clusters. To arrive at the final cluster count rates in each filter, this mean background level was multiplied by the number of pixels in a given source aperture and subtracted from the summed cluster counts within that aperture. Uncertainties for the final cluster magnitudes and colours were estimated by remeasuring cluster count rates through apertures centred on 4 distinct positions away by $3\,\sigma$ from the derived cluster centre and adding the formal uncertainty of the photometric calibration in quadrature. The final magnitudes and colours of the target clusters are listed for aperture radii of $30''$, $45''$, $60''$, and $100''$ in Table A1 (in the Appendix). Magnitudes and colours for other radii can be provided by the first author on request.

3.2 Comparison with previous studies

We obtain an external measure of the accuracy of our measurements by comparing our results with previous studies. As we found no prior integrated photometry in the R– and I-bands for our LMC clusters in the literature, we limit this comparison to one with V magnitudes from the large compilation of integrated UBV photometry by van den Bergh

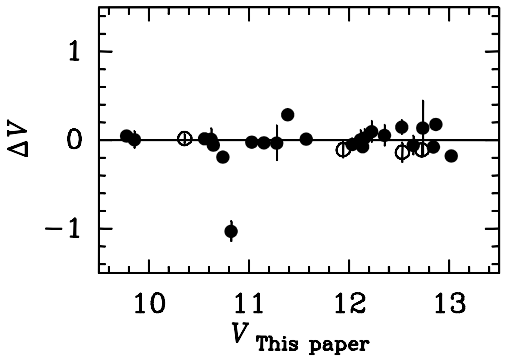

Figure 1. Comparison of our V magnitudes with those from van den Bergh (1981). The difference ΔV is in the sense "our values minus those of van den Bergh". Filled circles represent data take during the Jan 2002 observing run, open circles represent data taken during the Dec 2004 run. The errorbars only represent our uncertainties, since the data in van den Bergh (1981) do not contain photometric uncertainties. The solid line represents $\Delta V = 0$.

(1981), which contains V-band data for all clusters in our sample. This comparison is shown in Figure 1. We derived V magnitudes for our data using the aperture radii listed in Tables 2 and 3 of van den Bergh (1981) for the purpose of this comparison. As van den Bergh did not provide photometric uncertainties for the data he compiled, the error bars plotted in Figure 1 only reflect our uncertainties. In any case, it can be seen that the data agree very well with each other. The formal difference in V magnitudes, $\Delta V \equiv V_{\rm this\ paper} - V_{\rm van\ den\ Bergh} = -0.03 \pm 0.04$ where the error estimate represents the mean error of the mean. There is one outlier, which is the young cluster NGC 2058, where we measure a significantly brighter V magnitude than van den Bergh. NGC 2058 is located in a rather crowded region of the LMC with significant variations in the surface brightness of the field population outside the cluster. It is also surrounded by neighbouring clusters. To understand this discrepancy, we investigated three possibilities: *(i)* An unfortunate miscentering of the aperture used by the single-channel photometry reported in van den Bergh (1981), which might have been the case if the aperture was centered using a blue-sensitive eyepiece at the time (single bright young stars located off the cluster centre might cause such an effect; see Pessev et al. (2006) for illustrations of this effect in the near-IR). However, in order to arrive at van den Bergh's V magnitude, we find that one would have to locate the aperture $\sim 32''$ off the cluster centre, which is half the diameter of the van den Bergh aperture. This seems unlikely, but cannot be ruled out a priori. *(ii)* An unfortunate placement of the background aperture of the measurement of NGC 2058 in van den Bergh's compilation onto a neighbouring (e.g., faint) star cluster. However, we could only account for an error of 0.45 mag that way (placing the background aperture centered on the brightest neighbouring cluster on the CCD), which is still 0.55 mag short of explaining the discrepancy. *(iii)* An unfortunate error in our photometric calculations. However, we did double-check our measurements, and the V-band magnitudes of all other clusters observed during the same night (for which the photometry was derived in the exact same way as for NGC 2058) *are* consistent with those listed in van den Bergh (1981). We conclude that in the absence of knowledge of the location of the object and background apertures for NGC 2058 in the van den Bergh (1981) compilation, it is impossible to pinpoint the reason for this discrepancy. For now, we suggest that it may be at least partly due to aperture miscentering and/or unfortunate background aperture placement as described above.

For the SMC clusters in our sample, we compare our V magnitudes and $V-I$ colours with those measured by the recent CCD imaging study of Rafelski & Zaritsky (2005, hereafter RZ05) in Fig. 2. As RZ05 used cluster radii from Hill & Zaritsky (2006) for their *UBVI* measurements, we did so too for this comparison. The agreement in both V magnitudes and $V-I$ colours is within the uncertainties, which is encouraging since they used a similar measurement method. The formal differences in V magnitudes and $V-I$ colours are $\Delta V \equiv V_{\rm this\ paper} - V_{\rm RZ05} = -0.06 \pm 0.03$ and $\Delta(V-I) \equiv (V-I)_{\rm this\ paper} - (V-I)_{\rm RZ05} = -0.01 \pm 0.01$, respectively, where the error estimates represent the mean error of the mean. The average errors of the ΔV and $\Delta(V$–$I)$ values themselves are 0.34 mag and 0.12 mag, respectively.

3.3 Extinction Corrections

Cluster extinction values were obtained from two independent studies: Schlegel, Finkbeiner, & Davis (1998), and Zaritsky et al. (2002; 2004). While the Schlegel et al. (1998) measurements cover the whole sky and use direct measurements of dust emission, it has been recognized that their extinction maps are rather uncertain in the inner regions of the Magellanic Clouds due to the lack of adequate temperature structure resolution by DIRBE and the fact that their extinction values might be systematically underestimated due to the possible presence of cold dust invisible to IRAS. With this in mind, our adopted extinction values were determined primarily from the measurements of Zaritsky et al. (2002; 2004) which are based on stellar atmosphere model fits to *UBVI* photometry of thousands of individual stars across the SMC and LMC. We chose to derive extinction values from the "cool" stars ($T_{\rm eff} < 10^4$ K) in the Zaritsky et al. surveys. This choice was made after considering that *(i)* our objects are all significantly older than 10 Myr, and *(ii)* the U-band photometry from Zaritsky et al. is significantly less deep than their B, V, and I-band photometry, rendering their stellar atmosphere model fitting procedure to be typically more precise for cooler stars. The clusters were assigned an extinction value that is the mean of the distribution of values returned by the Zaritsky et al. method, while its uncertainty was assigned the mean error of that mean value. We ended up using a search radius of $5'$ around the center coordinates of the target star clusters, as the use of smaller search radii sometimes returned rather few stars with extinction estimates. From experimentation with different values of the search radius, we estimate the systematic uncertainty of the A_V extinction values listed in Table 1 to be within 0.02 mag. For those target clusters not covered by the Zaritsky et al. surveys (whose A_V values are indicated with asterisk superscripts in Table 1), we use extinction values from Schlegel et al. (1998) and correct them to the Zaritsky et al. extinction scale by adding the mean difference of A_V values for clusters for which both extinction values are available. This mean difference was determined

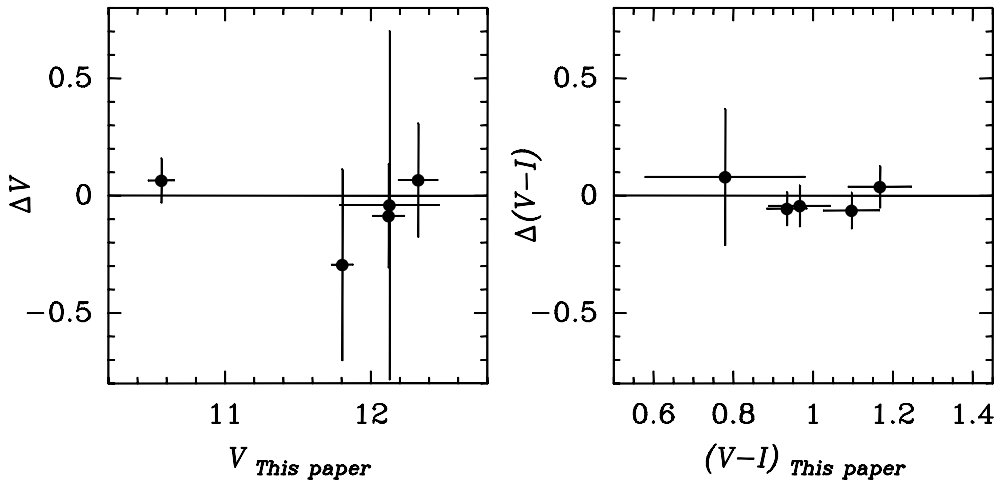

Figure 2. Comparison of our magnitudes and colours with those from Rafelski & Zaritsky (2005) for the clusters in common between the two studies (NGC 152, NGC 265, NGC 339, NGC 411, and NGC 419). V magnitudes are compared in the left panel, and $V-I$ colours are compared in the right panel. The differences ΔV and $\Delta(V-I)$ are in the sense "our values minus those of Rafelski & Zaritsky". The solid lines represent $\Delta V = 0$ (left panel) and $\Delta(V-I) = 0$ (right panel).

to be $A_{V,\,\mathrm{Zaritsky\ et\ al.}} - A_{V,\,\mathrm{Schlegel\ et\ al.}} = 0.02 \pm 0.01$. Uncertainties of extinction values derived from Schlegel et al. (1998) were assigned the mean uncertainty of the extinction values derived from the Zaritsky et al. surveys in the SMC or LMC, depending on the cluster in question, with the 0.01 mag of uncertainty mentioned above added in quadrature. The conversion of A_V values to A_R and A_I was done using the formulae in Cardelli, Clayton, & Mathis (1989) with $R_V = 2.7$ and 3.4 for the SMC and LMC, respectively (Gordon et al. 2003). We used reference wavelengths of 6407 Å and 7982 Å for the Kron-Cousins R and I bands, respectively (Bessell 1990). The final extinction values are listed in Table 1. Dereddened cluster colours $(V-R)_0$ and $(V-I)_0$ are listed in Table A1.

4 CONCLUDING REMARKS

We have presented accurate integrated-light photometry in Johnson/Cousins V, R, and I for a sample of 28 globular clusters in the Magellanic Clouds, most of which have reliable age and metallicity estimates available in the literature. The sample encompasses estimated ages between 50 Myr and 7 Gyr, and metallicities ([Fe/H]) between −1.50 and +0.01 dex. The sample is dominated by clusters of ages between roughly 0.5 and 2 Gyr, an age range during which the bolometric luminosity of simple stellar populations is dominated by AGB stars whose theoretical colours are rather uncertain. Hence, an empirical calibration of the colours of SSPs during this age range is important. Indeed, the data presented here have recently been used by Maraston (2005) to update the calibration of SSP models, finding that the influence of AGB effects is significant in R and I. To our knowledge, this is the first study to present R-band photometry for any cluster in our sample, and I-band photometry for any LMC cluster.

Acknowledgments.
This work is based on observations obtained at the Cerro Tololo Interamerican Observatory, which is is operated by the Association of Universities for Research in Astronomy (AURA), Inc., under contract to the U. S. National Science Foundation. This research has made use of the NASA/IPAC Extragalactic Database (NED) which is operated by the Jet Propulsion Laboratory, California Institute of Technology, under contract with the National Aeronautics and Space Administration. We thank CTIO staff observer Arturo Gomez for his help in securing the observations of the December 2004 run operated by the SMARTS consortium. We acknowledge helpful discussions with Peter Pessev, and thank the anonymous referee for a fast and thorough review of this paper. PG and DG also thank the Director of STScI for funding part of this research through a director's discretionary research grant.

REFERENCES

Bessell, M. S., 1990, PASP, 102, 1181
Bica, E., Clariá, J. J., Dottori, H., Santos, J. F. C. Jr., & Piatti, A. E., 1996, ApJS, 102, 57
Bica, E., Schmitt, H. R., Dutra, C. M., & Oliveira, H. L. 1999, AJ, 117, 238
Bruzual, G. A., & Charlot, S., 2003, MNRAS, 344, 1000
Cardelli, J. A., Clayton, G. C., & Mathis, J. S. 1989, ApJ, 345, 245
Cohen, J. G., 1982, ApJ, 258, 143
Cohen, J. G., Frogel, J. A., Persson, S. E., Elias, J. H. 1981, ApJ, 249, 481
Crowl, H. H., Sarajedini, A., Piatti, A. E., Geisler, D., Bica, E., Clariá, J. J., & Santos, J. F. C. 2001, AJ, 122, 220
Da Costa, G. S., & Hatzidimitriou, D. 1998, AJ, 115, 1934
Dirsch, B., Richtler, T., Gieren, W. P., & Hilker, M. 2000, A&A, 360, 133
Durand, D., Hardy, E., & Melnick, J. 1984, ApJ, 283, 552
Elson, R. A. W., 1991, ApJS, 76, 185
Elson, R. A. W., Fall, S. M. 1985, PASP, 97, 692
Elson, R. A. W., Fall, S. M. 1988, AJ, 96, 1383
Ferraro, F. R., Fusi Pecci, F., Testa, V., Greggio, L., Corsi,

C. E., Buonanno, R., Terndrup, D. M., & Zinnecker, H., 1995, MNRAS, 272, 391
Ferraro, F. R., Origlia, L., Testa, V., & Maraston, C., 2004, ApJ, 608, 772
Frogel, J. A., Mould, J. R., Blanco, V. M. 1990, ApJ, 352, 96
Geisler, D., Bica, E., Dottori, H., Claria, J. J., Piatti, A. E., & Santos, J. F. C. 1997, AJ, 114, 1920
Girardi, L., Choisi, C., Bertelli, G., & Bressan, A., 1995, A&A, 298, 87
Girardi, L., & Bertelli, G. 1998, MNRAS, 300, 533
Gordon, K. D., Clayton, G. C., Misselt, K. A., Landolt, A. U., & Wolff, M. J. 2003, ApJ, 594, 279
Goudfrooij, P., Mack, J., Kissler–Patig, M., Meylan, G., & Minniti, D. 2001a, MNRAS, 322, 643
Goudfrooij, P., Alonso, M. V., Maraston, C., & Minniti, D. 2001b, MNRAS, 328, 237
Hill, A., & Zaritsky, D. 2006, AJ, 131, 414
Hill, V., François, P., Spite, M., Primas, F., & Spite, F. 2000, A&A, 364, L19
Hodge, P. W. 1984, PASP, 96, 947
Hunter, D. A., Shaya, E. J., Holtzman, J. A., Light, R. M., O'Neil, E. J., & Lynds, R. 1995, ApJ, 448, 179
Iben, I., Jr., & Renzini, A., ARA&A, 21, 271
Lançon, A. 1999, in Le Bertre T., Lebre A., Waelkens C., Asymptotic Giant Branch Stars. Kluwer, Dordrecht, p. 579
Landolt, A. U. 1992, AJ, 104, 340
Maraston, C., 1998, MNRAS, 300, 872
Maraston, C., 2004, in Bender, R., Renzini, A., Multi-wavelength Mapping of Galaxy Formation and Evolution. Springer, Berlin, p. 290
Maraston, C., 2005, MNRAS, 362, 799
Maraston, C., Kissler-Patig, M., Brodie, J. P., Barmby, P., & Huchra, J. P. 2001, A&A, 370, 176
Marigo, P., 2001, A&A, 370, 194
Massey, P. 2002, ApJS, 141, 81
Mighell, K. J., Sarajedini, A., & French, R. S. 1998, ApJ, 494, L189
Minniti, D., Alonso, M. V., Goudfrooij, P., Jablonka, P., & Meylan, G. 1996, ApJ, 467, 221
Olszewski, E. W., Schommer, R. A., Suntzeff, N. B., & Harris, H. C. 1991, AJ, 101, 515
Persson, S. E., Aaronson, M., Cohen, J. G., Frogel, J. A., Mathews, K. 1983, ApJ, 266, 105
Pessev, P. M., Goudfrooij, P., Puzia, T. H., & Chandar, R. 2006, submitted to AJ
Rafelski, M., & Zaritsky, D., 2005, AJ, 129, 2701
Renzini, A., 1992, in Barbuy B., Renzini A., eds, Proc. IAU Symp. 149, The Stellar Populations of Galaxies. Kluwer, Dordrecht, p. 325
Renzini, A., & Buzzoni, A., 1986, in Chiosi C., Renzini A., eds, Spectral Evolution of Galaxies. Reidel, Dordrecht, p. 195
Renzini, A., & Voli, M., 1981, A&A, 94, 175
Rich, R. M., Shara, M. M., & Zurek, D. 2001, AJ, 122, 842
Sagar, R., & Pandey, A. K., 1989, A&AS, 79, 407
Schlegel, D. J., Finkbeiner, D. P., Davis, M., 1998, ApJ, 500, 525
Schmidt-Kaler, Th., 1982, in Schaifers K., Voigt H. E., eds, Landolt-Börnstein: Numerical Data and Functional Relationships in Science and Technology. Springer–Verlag, Berlin, VI/2b
Schommer, R. A., & Geisler, D. 1988, in Grindlay, J. E. & Davis Philip, A. G., eds, IAU Symp. No. 126, The Harlow-Shapley Symposium on Globular Cluster Systems in Galaxies, Reidel, Dordrecht, p. 577
Schweizer, F., Miller, B. W., Whitmore, B. C., & Fall, S. M., 1996, AJ, 112, 1839
Searle, L., Wilkinson, A., Bagnuolo, W. G., 1980, ApJ, 239, 803 (SWB)
Stetson, P. B., 1987, PASP, 99, 191
Udalski, A., 2000, Acta Astronomica, 50, 279
van den Bergh, S., 1981, A&AS, 46, 79
Wagenhuber, J., & Groenewegen, M. A. T., 1998, A&A, 340, 183
Welch, D. L. 1991, AJ, 101, 538
Whitmore, B. C., Schweizer, F., Leitherer, C., Borne, K., & Robert, C., 1993, AJ, 106, 1354
Zaritsky, D., Harris, J., Thompson, I. B., Grebel, E. K., & Massey, P. 2002, AJ, 123, 855
Zaritsky, D., Harris, J., Thompson, I. B., & Grebel, E. K. 2004, AJ, 128, 1606

APPENDIX A: APERTURE PHOTOMETRY OF 28 GLOBULAR CLUSTERS IN THE MAGELLANIC CLOUDS

Table A1. *VRI* Photometry of globular clusters in the Magellanic clouds.

Object	Aperture Radius*	V [mag]	$V-R$ [mag]	$V-I$ [mag]	$(V-R)_0$ [mag]	$(V-I)_0$ [mag]
			SMC Clusters			
Kron 3	30	13.049 ± 0.048		0.943 ± 0.063		0.873 ± 0.063
	45	12.313 ± 0.051		0.994 ± 0.066		0.924 ± 0.066
	60	11.933 ± 0.057		0.978 ± 0.074		0.908 ± 0.074
	100	11.411 ± 0.085		0.995 ± 0.107		0.925 ± 0.107
NGC 152	30	14.085 ± 0.026	0.476 ± 0.033	1.041 ± 0.032	0.446 ± 0.033	0.967 ± 0.033
	45	13.243 ± 0.026	0.547 ± 0.033	1.117 ± 0.033	0.517 ± 0.033	1.043 ± 0.034
	60	12.820 ± 0.031	0.593 ± 0.038	1.208 ± 0.037	0.562 ± 0.038	1.134 ± 0.038
	100	12.327 ± 0.053	0.570 ± 0.064	1.168 ± 0.063	0.540 ± 0.064	1.094 ± 0.064
NGC 265	30	12.735 ± 0.034	0.259 ± 0.069	0.567 ± 0.078	0.227 ± 0.069	0.490 ± 0.078
	45	12.299 ± 0.048	0.336 ± 0.097	0.737 ± 0.101	0.304 ± 0.097	0.660 ± 0.101
	60	12.176 ± 0.074	0.333 ± 0.152	0.721 ± 0.160	0.301 ± 0.152	0.643 ± 0.160
	100	12.020 ± 0.174	0.292 ± 0.374	0.621 ± 0.412	0.260 ± 0.374	0.544 ± 0.412
NGC 339	30	13.942 ± 0.037		0.912 ± 0.052		0.842 ± 0.053
	45	13.162 ± 0.038		0.961 ± 0.052		0.891 ± 0.053
	60	12.720 ± 0.039		0.975 ± 0.053		0.905 ± 0.054
	100	12.124 ± 0.044		0.967 ± 0.060		0.897 ± 0.061
NGC 411	30	12.944 ± 0.035	0.597 ± 0.050	0.946 ± 0.049	0.570 ± 0.050	0.880 ± 0.049
	45	12.484 ± 0.039	0.586 ± 0.054	0.957 ± 0.052	0.559 ± 0.054	0.891 ± 0.052
	60	12.191 ± 0.044	0.562 ± 0.061	0.914 ± 0.059	0.535 ± 0.061	0.848 ± 0.059
	100	11.806 ± 0.067	0.543 ± 0.091	0.874 ± 0.086	0.516 ± 0.091	0.808 ± 0.086
NGC 419	30	11.311 ± 0.038	0.529 ± 0.039	1.052 ± 0.040	0.478 ± 0.040	0.928 ± 0.041
	45	10.850 ± 0.055	0.533 ± 0.056	1.053 ± 0.057	0.482 ± 0.056	0.929 ± 0.058
	60	10.595 ± 0.076	0.542 ± 0.077	1.069 ± 0.079	0.491 ± 0.077	0.944 ± 0.080
	100	10.304 ± 0.161	0.571 ± 0.162	1.097 ± 0.166	0.520 ± 0.162	0.972 ± 0.166
			LMC Clusters			
NGC 1644	30	13.184 ± 0.012	0.407 ± 0.016	0.811 ± 0.020	0.363 ± 0.017	0.702 ± 0.022
	45	12.922 ± 0.016	0.417 ± 0.020	0.838 ± 0.028	0.373 ± 0.020	0.729 ± 0.029
	60	12.824 ± 0.022	0.416 ± 0.027	0.835 ± 0.043	0.371 ± 0.027	0.726 ± 0.043
	100	12.665 ± 0.048	0.419 ± 0.057	0.836 ± 0.097	0.375 ± 0.057	0.727 ± 0.097
NGC 1651	30	13.332 ± 0.047		0.879 ± 0.065		0.743 ± 0.068
	45	12.769 ± 0.055		0.896 ± 0.075		0.760 ± 0.078
	60	12.506 ± 0.069		0.896 ± 0.093		0.760 ± 0.096
	100	12.132 ± 0.122		1.147 ± 0.151		1.011 ± 0.154
NGC 1751	30	12.911 ± 0.039	0.599 ± 0.055	1.324 ± 0.045	0.517 ± 0.055	1.126 ± 0.046
	45	12.378 ± 0.051	0.636 ± 0.072	1.349 ± 0.059	0.554 ± 0.072	1.151 ± 0.059
	60	12.088 ± 0.069	0.652 ± 0.096	1.416 ± 0.077	0.570 ± 0.096	1.218 ± 0.077
	100	11.669 ± 0.127	0.608 ± 0.183	1.343 ± 0.143	0.526 ± 0.183	1.145 ± 0.143
NGC 1755	30	10.239 ± 0.022	0.216 ± 0.024	0.504 ± 0.026	0.130 ± 0.025	0.295 ± 0.028
	45	9.969 ± 0.031	0.202 ± 0.033	0.482 ± 0.035	0.115 ± 0.034	0.272 ± 0.036
	60	9.859 ± 0.047	0.193 ± 0.048	0.470 ± 0.049	0.106 ± 0.048	0.260 ± 0.050
	100	9.723 ± 0.109	0.168 ± 0.111	0.440 ± 0.111	0.081 ± 0.111	0.230 ± 0.112
NGC 1783	30	11.833 ± 0.015	0.474 ± 0.020	1.020 ± 0.095	0.424 ± 0.021	0.900 ± 0.095
	45	11.238 ± 0.017	0.476 ± 0.024	1.010 ± 0.124	0.426 ± 0.024	0.890 ± 0.124
	60	10.896 ± 0.021	0.475 ± 0.028	1.015 ± 0.159	0.426 ± 0.029	0.895 ± 0.160
	100	10.393 ± 0.034	0.485 ± 0.045	1.078 ± 0.262	0.435 ± 0.045	0.958 ± 0.262
NGC 1806	30	12.185 ± 0.040	0.689 ± 0.053	1.386 ± 0.052	0.649 ± 0.053	1.289 ± 0.052
	45	11.672 ± 0.040	0.669 ± 0.053	1.335 ± 0.053	0.629 ± 0.053	1.238 ± 0.053
	60	11.374 ± 0.041	0.667 ± 0.055	1.338 ± 0.055	0.627 ± 0.055	1.241 ± 0.055
	100	10.999 ± 0.046	0.669 ± 0.063	1.344 ± 0.065	0.629 ± 0.063	1.247 ± 0.065
NGC 1831	30	11.964 ± 0.021	0.274 ± 0.032	0.539 ± 0.037	0.212 ± 0.033	0.388 ± 0.038
	45	11.382 ± 0.026	0.301 ± 0.040	0.613 ± 0.046	0.239 ± 0.041	0.461 ± 0.046
	60	11.094 ± 0.035	0.302 ± 0.054	0.641 ± 0.060	0.239 ± 0.054	0.490 ± 0.060
	100	10.729 ± 0.067	0.288 ± 0.104	0.630 ± 0.117	0.225 ± 0.104	0.479 ± 0.117
NGC 1846	30	12.349 ± 0.086	0.544 ± 0.087	1.094 ± 0.089	0.472 ± 0.087	0.919 ± 0.089
	45	11.672 ± 0.104	0.551 ± 0.105	1.155 ± 0.107	0.479 ± 0.105	0.980 ± 0.107
	60	11.262 ± 0.126	0.563 ± 0.127	1.214 ± 0.129	0.491 ± 0.127	1.040 ± 0.129
	100	10.675 ± 0.203	0.532 ± 0.205	1.166 ± 0.208	0.460 ± 0.205	0.992 ± 0.209

Note to Table A1: * Radii are given in arcseconds.

Table A1. (continued)

Object	Aperture Radius*	V [mag]	$V-R$ [mag]	$V-I$ [mag]	$(V-R)_0$ [mag]	$(V-I)_0$ [mag]
NGC 1866	30	10.642 ± 0.010	0.331 ± 0.015	0.641 ± 0.015	0.289 ± 0.015	0.540 ± 0.017
	45	10.128 ± 0.010	0.322 ± 0.015	0.618 ± 0.015	0.281 ± 0.015	0.517 ± 0.017
	60	9.873 ± 0.011	0.308 ± 0.016	0.593 ± 0.017	0.266 ± 0.016	0.493 ± 0.018
	100	9.533 ± 0.013	0.319 ± 0.021	0.650 ± 0.022	0.278 ± 0.021	0.549 ± 0.023
NGC 1868	30	11.917 ± 0.017	0.360 ± 0.022	0.786 ± 0.023	0.298 ± 0.022	0.635 ± 0.024
	45	11.643 ± 0.020	0.350 ± 0.027	0.764 ± 0.026	0.287 ± 0.027	0.612 ± 0.028
	60	11.528 ± 0.027	0.342 ± 0.037	0.758 ± 0.033	0.279 ± 0.037	0.606 ± 0.034
	100	11.382 ± 0.056	0.328 ± 0.080	0.760 ± 0.065	0.266 ± 0.080	0.608 ± 0.066
NGC 1978	30	11.548 ± 0.011	0.574 ± 0.016	1.135 ± 0.016	0.486 ± 0.017	0.922 ± 0.019
	45	10.930 ± 0.012	0.570 ± 0.017	1.108 ± 0.016	0.482 ± 0.018	0.894 ± 0.020
	60	10.616 ± 0.014	0.552 ± 0.019	1.073 ± 0.018	0.464 ± 0.019	0.860 ± 0.021
	100	10.203 ± 0.020	0.557 ± 0.027	1.088 ± 0.025	0.469 ± 0.028	0.875 ± 0.028
NGC 1987	30	12.626 ± 0.021	0.422 ± 0.028	0.964 ± 0.032	0.369 ± 0.029	0.836 ± 0.033
	45	12.249 ± 0.031	0.412 ± 0.042	0.912 ± 0.049	0.359 ± 0.042	0.784 ± 0.049
	60	12.000 ± 0.042	0.456 ± 0.056	1.026 ± 0.063	0.403 ± 0.056	0.897 ± 0.064
	100	11.744 ± 0.090	0.441 ± 0.121	0.982 ± 0.139	0.389 ± 0.121	0.854 ± 0.139
NGC 2058	30	11.219 ± 0.018	0.267 ± 0.025	0.615 ± 0.029	0.228 ± 0.025	0.522 ± 0.030
	45	10.912 ± 0.022	0.258 ± 0.033	0.596 ± 0.040	0.220 ± 0.033	0.503 ± 0.041
	60	10.732 ± 0.028	0.248 ± 0.045	0.576 ± 0.057	0.210 ± 0.046	0.483 ± 0.057
	100	10.451 ± 0.053	0.251 ± 0.091	0.639 ± 0.110	0.213 ± 0.091	0.546 ± 0.110
NGC 2134	30	11.521 ± 0.011	0.264 ± 0.016	0.572 ± 0.017	0.185 ± 0.016	0.382 ± 0.018
	45	11.158 ± 0.013	0.263 ± 0.018	0.572 ± 0.020	0.185 ± 0.019	0.382 ± 0.021
	60	10.972 ± 0.017	0.262 ± 0.023	0.563 ± 0.025	0.184 ± 0.023	0.373 ± 0.026
	100	10.742 ± 0.031	0.295 ± 0.042	0.663 ± 0.047	0.217 ± 0.042	0.473 ± 0.047
NGC 2136	30	11.059 ± 0.012	0.327 ± 0.016	0.728 ± 0.016	0.254 ± 0.016	0.549 ± 0.018
	45	10.715 ± 0.015	0.308 ± 0.019	0.683 ± 0.019	0.235 ± 0.019	0.505 ± 0.020
	60	10.500 ± 0.019	0.287 ± 0.023	0.642 ± 0.023	0.213 ± 0.023	0.463 ± 0.024
	100	10.295 ± 0.040	0.311 ± 0.044	0.684 ± 0.044	0.237 ± 0.044	0.505 ± 0.044
NGC 2154	30	12.810 ± 0.033	0.473 ± 0.044	1.005 ± 0.054	0.419 ± 0.044	0.873 ± 0.055
	45	12.329 ± 0.046	0.489 ± 0.060	1.067 ± 0.075	0.435 ± 0.061	0.935 ± 0.075
	60	12.099 ± 0.064	0.488 ± 0.085	1.060 ± 0.105	0.433 ± 0.085	0.928 ± 0.106
	100	11.851 ± 0.138	0.494 ± 0.184	1.137 ± 0.229	0.439 ± 0.184	1.005 ± 0.229
NGC 2155	30	13.417 ± 0.094	0.556 ± 0.104	1.007 ± 0.157	0.500 ± 0.104	0.872 ± 0.157
	45	12.909 ± 0.132	0.581 ± 0.145	1.030 ± 0.217	0.525 ± 0.145	0.894 ± 0.218
	60	12.696 ± 0.193	0.601 ± 0.211	1.006 ± 0.322	0.545 ± 0.211	0.871 ± 0.322
	100	12.593 ± 0.485	0.680 ± 0.524	0.906 ± 0.863	0.624 ± 0.524	0.770 ± 0.863
NGC 2162	30	13.284 ± 0.045	0.535 ± 0.051	1.087 ± 0.055	0.472 ± 0.051	0.935 ± 0.043
	45	12.846 ± 0.065	0.563 ± 0.073	1.122 ± 0.078	0.501 ± 0.073	0.971 ± 0.058
	60	12.613 ± 0.092	0.535 ± 0.103	1.064 ± 0.112	0.472 ± 0.104	0.912 ± 0.081
	100	12.350 ± 0.198	0.563 ± 0.221	1.087 ± 0.240	0.500 ± 0.221	0.936 ± 0.167
NGC 2164	30	10.774 ± 0.033		0.312 ± 0.046		0.153 ± 0.053
	45	10.490 ± 0.033		0.332 ± 0.046		0.173 ± 0.053
	60	10.309 ± 0.033		0.370 ± 0.046		0.211 ± 0.053
	100	10.105 ± 0.033		0.386 ± 0.047		0.227 ± 0.054
NGC 2173	30	12.999 ± 0.037	0.573 ± 0.064	1.269 ± 0.055	0.511 ± 0.064	1.117 ± 0.056
	45	12.481 ± 0.050	0.573 ± 0.087	1.230 ± 0.073	0.510 ± 0.088	1.078 ± 0.074
	60	12.306 ± 0.074	0.558 ± 0.131	1.218 ± 0.108	0.496 ± 0.131	1.066 ± 0.109
	100	12.007 ± 0.224	0.540 ± 0.277	1.207 ± 0.225	0.477 ± 0.277	1.056 ± 0.225
NGC 2213	30	12.975 ± 0.019	0.575 ± 0.023	1.155 ± 0.023	0.504 ± 0.024	0.984 ± 0.025
	45	12.585 ± 0.027	0.600 ± 0.032	1.184 ± 0.032	0.530 ± 0.032	1.013 ± 0.033
	60	12.477 ± 0.042	0.596 ± 0.049	1.170 ± 0.048	0.526 ± 0.049	0.999 ± 0.049
	100	12.365 ± 0.102	0.640 ± 0.116	1.225 ± 0.115	0.570 ± 0.116	1.054 ± 0.115
NGC 2231	30	13.648 ± 0.016	0.562 ± 0.026	1.073 ± 0.090	0.500 ± 0.026	0.921 ± 0.090
	45	13.231 ± 0.020	0.541 ± 0.034	1.002 ± 0.139	0.479 ± 0.034	0.851 ± 0.139
	60	13.206 ± 0.021	0.539 ± 0.034	0.995 ± 0.143	0.477 ± 0.034	0.844 ± 0.143
	100	12.655 ± 0.055	0.517 ± 0.095	0.779 ± 0.517	0.455 ± 0.095	0.627 ± 0.517

Note to Table: * Radii are given in arcseconds.